


# Real-space dynamical mean field theory study of non-Hermitian skin effect for correlated systems: Analysis based on pseudospectrum

Tsuneya Yoshida *Department of Physics, University of Tsukuba, Ibaraki 305-8571, Japan*

(Received 10 November 2020; accepted 16 February 2021; published 23 March 2021)

We analyze a correlated system in equilibrium with special emphasis on non-Hermitian topology inducing a skin effect. The pseudospectrum, computed by the real-space dynamical mean field theory, elucidates that additional pseudoeigenstates emerge for the open boundary condition in contrast to the dependence of the density of states on the boundary condition. We further discuss how the line-gap topology, another type of non-Hermitian topology, affects the pseudospectrum. Our numerical simulation clarifies that while the damping of the quasiparticles induces the nontrivial point-gap topology, it destroys the nontrivial line-gap topology. The above two effects are also reflected in the temperature dependence of the local pseudospectral weight.

DOI: [10.1103/PhysRevB.103.125145](https://doi.org/10.1103/PhysRevB.103.125145)

## I. INTRODUCTION

In these decades, topological properties of condensed matters enhance their significance [1–7]. Among a variety of topological systems, recently, non-Hermitian systems attract broad interest because of their unique topological phenomena induced by non-Hermiticity [8–22]. Representative examples of non-Hermitian topological phenomena are the emergence of exceptional points [23–29] and a skin effect [11,30–42]. The former is non-Hermitian topological band touching points in the bulk on which the Hamiltonian becomes nondiagonalizable. The latter results in extreme sensitivity to the boundary conditions. The platform of non-Hermitian topology extends to a wide range of systems with gain and loss, e.g., photonic crystals [43–50], open quantum systems [11,24,51–59], mechanical metamaterials [60–62], electric circuits [63–65], and so on.

As well as the above dissipative systems, the non-Hermitian topology also provides a novel perspective of strongly correlated systems in equilibrium [66,67]. In such a system, the single-particle spectrum is described by an effective non-Hermitian Hamiltonian which is composed of the noninteracting Hamiltonian and the self-energy [21,27,66–76]. So far, it has been elucidated that exceptional points induce the bulk Fermi arc in the single-particle spectrum for equilibrium correlated systems.

Despite the above progress of non-Hermitian band touching in the bulk, other topological properties inducing the skin effect have not been sufficiently explored in correlated systems. Although Okuma and Sato proposed that the topological properties of the skin effect are accessible by the pseudospectrum [77], an explicit numerical simulation of correlated systems is still missing. In particular, it remains unclear in which correlated system the effective Hamiltonian possesses topological properties of the skin effect.

In this paper, by employing the real-space dynamical mean field theory (R-DMFT), we analyze a two-dimensional cor-

related lattice model in equilibrium with special emphasis on the non-Hermitian topology of the skin effect. Our R-DMFT simulation demonstrates that the nontrivial point-gap topology of the skin effect induces additional pseudoeigenstates in contrast to the dependence of the density of states (DOS) on the boundary condition [for definition of the point-gap, see Eq. (7)]. We also elucidate how the line-gap topology, another type of non-Hermitian topology, affects the pseudospectrum [for a definition of the line gap, see Eq. (8)]. Our analysis clarifies that the damping of the quasiparticles has two effects; it induces the nontrivial point-gap topology and destroys the nontrivial line-gap topology. The above two effects result in distinct temperature dependences of the local pseudospectral weight depending on the momentum  $k_x$ ; for  $k_x = 0$ , the temperatures suppress the dependence of the local pseudospectral weight on the boundary conditions in contrast to the case for  $k_x = \pi/2$ .

The rest of this paper is organized as follows. In Sec. II, we define the correlated model where the effective Hamiltonian shows the skin effect. In this section, we also describe the framework of the R-DMFT and how to numerically extract the pseudospectrum from the R-DMFT data. The R-DMFT results are presented in Sec. III. In Appendices A and B, we briefly review several properties of the pseudospectrum.

## II. MODEL AND METHOD

### A. Two-orbital correlated model

We analyze the following Hamiltonian,

$$H = \sum_{(ij)\alpha\beta\sigma} h_{i\alpha j\beta} c_{i\alpha\sigma}^\dagger c_{j\beta\sigma} + U \sum_i \left( n_{i\uparrow} - \frac{1}{2} \right) \left( n_{i\downarrow} - \frac{1}{2} \right), \quad (1)$$

where  $c_{j\beta\sigma}^\dagger$  ( $c_{j\beta\sigma}$ ) creates (annihilates) a fermion with a spin state  $\sigma = \uparrow, \downarrow$  in orbital  $\alpha = a, b$  at site  $i$ . The matrix element  $h_{i\alpha j\beta} \in \mathbb{C}$  is defined such that the Bloch Hamiltonian is

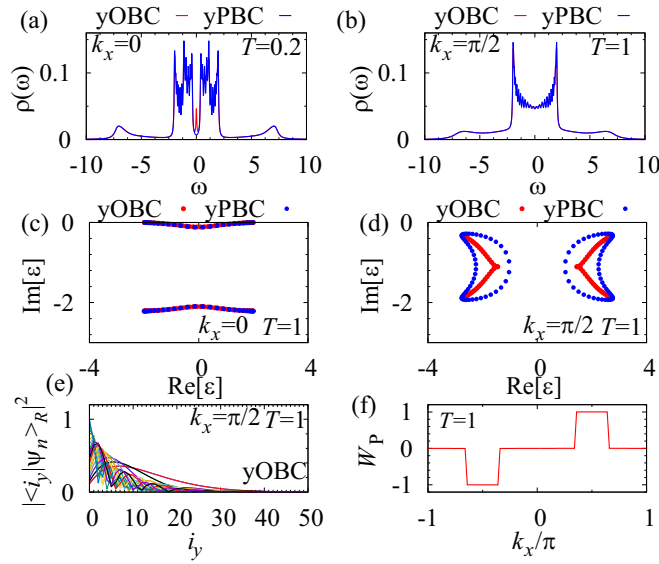


FIG. 1. (a) [(b)] Density of states  $\rho(\omega, k_x) = \frac{1}{L_y} \sum_{i_y, \alpha} [G(\omega, k_x)]_{i_y \alpha i_y \alpha}$  for  $(k_x, T) = (0, 0.2)$  [ $(\pi/2, 1)$ ]. (c) [(d)] Spectrum of  $\hat{H}_{\text{eff}}(0, k_x)$  for  $k_x = 0$  [ $\pi/2$ ]. The data represented with red (blue) dots are obtained by imposing the yOBC (yPBC). (e) Amplitude of right eigenvectors  $|\langle i_y | \psi_n \rangle_R|$  for  $k_x = \pi/2$ . (f) Winding number  $W_P(k_x)$ . These figures are obtained for  $U = 8$ . Panels (c)–(f) are obtained for  $T = 1$ .

written as

$$\hat{h}(\mathbf{k}) = t(2 \sin k_x - 0.5 \sin k_y) \hat{t}_2 + t(2 \cos k_y) \hat{t}_3. \quad (2)$$

Here, the matrices  $\tau$  are the Pauli matrices. The second term of Eq. (1) describes the repulsive interaction ( $U \geq 0$ ); the number operator for fermions is defined as  $n_{i\alpha\sigma} := c_{i\alpha\sigma}^\dagger c_{i\alpha\sigma}$ . Because the interaction is introduced as the second term of Eq. (1), the system is half-filled for arbitrary  $U$ .

We note that deviation of the self-energy of orbital  $a$  from the self-energy of orbital  $b$  is essential for non-Hermitian phenomena, which is realized by the imbalance of the interaction strength for orbital  $a$  and  $b$  [78,79]. It is also noted that the noninteracting model  $\hat{h}(\mathbf{k})$  is topologically identical to the tight-binding model of the honeycomb lattice which hosts Dirac cones [80]; the model has chiral symmetry, and the winding number takes 0 or 1 depending on the momentum (see Sec. III A). These topological properties are important for the nontrivial point-gap topology [see Figs. 2(c1)–2(c4)]. As a typical parameter set showing the same topology as the one of the honeycomb lattice model, we have chosen factors 2 and 0.5 in Eq. (2).

In this paper, we impose the periodic boundary condition along the  $x$  direction (xPBC). Along the  $y$  direction, we impose either open boundary conditions (yOBCs) or periodic boundary conditions (yPBCs). We note that  $t$  is taken as the energy unit ( $t = 1$ ).

## B. R-DMFT

Here, we briefly describe the R-DMFT, an extended version of the dynamical mean field theory [81–83], which allows us to treat systems with boundaries. To be concrete, let us

impose the xPBC and the yOBC on the model defined in Eq. (1). Here,  $i_y$  ( $i_y = 0, 1, \dots, L_y - 1$ ) labels the sites along the  $y$  direction. In such a case, the system is inhomogeneous along the  $y$  direction.

Within the R-DMFT framework, such inhomogeneity is encoded into the site-dependent self-energy  $\Sigma_{i_y b \sigma}$  which is computed by mapping the lattice model to a set of effective impurity models. The impurity model specified by  $i_y$  is written as

$$\mathcal{Z}_{\text{imp}, i_y} = \int \mathcal{D} \bar{d}_{i_y b \sigma} \mathcal{D} d_{i_y b \sigma} e^{-S_{\text{imp}, i_y}}, \quad (3a)$$

$$S_{\text{imp}, i_y} = - \int_0^\beta d\tau d\tau' \bar{d}_{i_y b \sigma}(\tau) \mathcal{G}_{i_y b \sigma}^{-1}(\tau - \tau') d_{i_y b \sigma}(\tau') + \int_0^\beta d\tau H_{\text{imp}, i_y} \delta(\tau), \quad (3b)$$

$$H_{\text{imp}, i_y} = U \left( n_{i_y b \uparrow} - \frac{1}{2} \right) \left( n_{i_y b \downarrow} - \frac{1}{2} \right). \quad (3c)$$

Here,  $\mathcal{Z}_{\text{imp}, i_y}$ ,  $S_{\text{imp}, i_y}$ , and  $H_{\text{imp}, i_y}$  denote a partition function, an effective action, and a local Hamiltonian of each impurity problem, respectively. The Grassmannian variables are denoted by  $\bar{d}_{i_y b \sigma}$  and  $d_{i_y b \sigma}$ .

The Green's functions of the effective bath  $\mathcal{G}_{i_y b \sigma}$  and the self-energy  $\Sigma_{i_y b \sigma}$  are obtained by self-consistently solving the above impurity models (3) and the following equations:

$$\mathcal{G}_{i_y b \sigma}^{-1} = G_{i_y b \sigma}^{-1} + \Sigma_{i_y b \sigma}, \quad (4a)$$

$$G_{i_y b \sigma} = \frac{1}{\sqrt{L_x}} \left[ \sum_{k_x} [(\omega + i\delta) \mathbb{1} - \hat{h}(k_x) - \hat{\Sigma}_\sigma(\omega)]^{-1} \right]_{i_y b i_y b}, \quad (4b)$$

with

$$\hat{\Sigma}_\sigma(\omega) = \text{diag}[0, \Sigma_{0b\sigma}(\omega + i\delta), 0, \Sigma_{1b\sigma}(\omega + i\delta), \dots]. \quad (4c)$$

Here,  $\hat{h}(k_x)$  is the Fourier-transformed Hamiltonian along the  $x$  direction for  $U = 0$ , and  $L_x$  denotes the number of sites along the  $x$  direction.

In order to compute the self-energy of effective impurity models, we have employed an iterative perturbation theory [84–86] based solver.

## C. Extracting the pseudospectrum from the R-DMFT data

The effective non-Hermitian Hamiltonian  $\hat{H}_{\text{eff}}(\omega, k_x) := \hat{h}(k_x) + \hat{\Sigma}(\omega)$  with the self-energy [see Eq. (4c)] may exhibit a non-Hermitian skin effect induced by the topological properties.

In Ref. [77], it has been proposed that the topological properties inducing the skin effect are accessible by the  $\epsilon$ -pseudospectrum ( $\epsilon > 0$ ) which can be measured by the angle-resolved photoemission spectroscopy [87]. In this section, we define the  $\epsilon$ -pseudo spectrum and describe how to compute it (for more details, see Appendices A and B).

The  $\epsilon$ -pseudospectrum  $\sigma_\epsilon[\hat{H}_{\text{eff}}(\omega, k_y)]$  with  $\epsilon > 0$  of the  $N \times N$  matrix  $\hat{H}_{\text{eff}}(\omega, k_y)$  is defined as a set of pseudoeigenvalues  $\eta \in \mathbb{C}$  satisfying

$$\|[\eta \mathbb{1} - \hat{H}_{\text{eff}}(\omega, k_y)]\mathbf{v}\| < \epsilon, \quad (5)$$

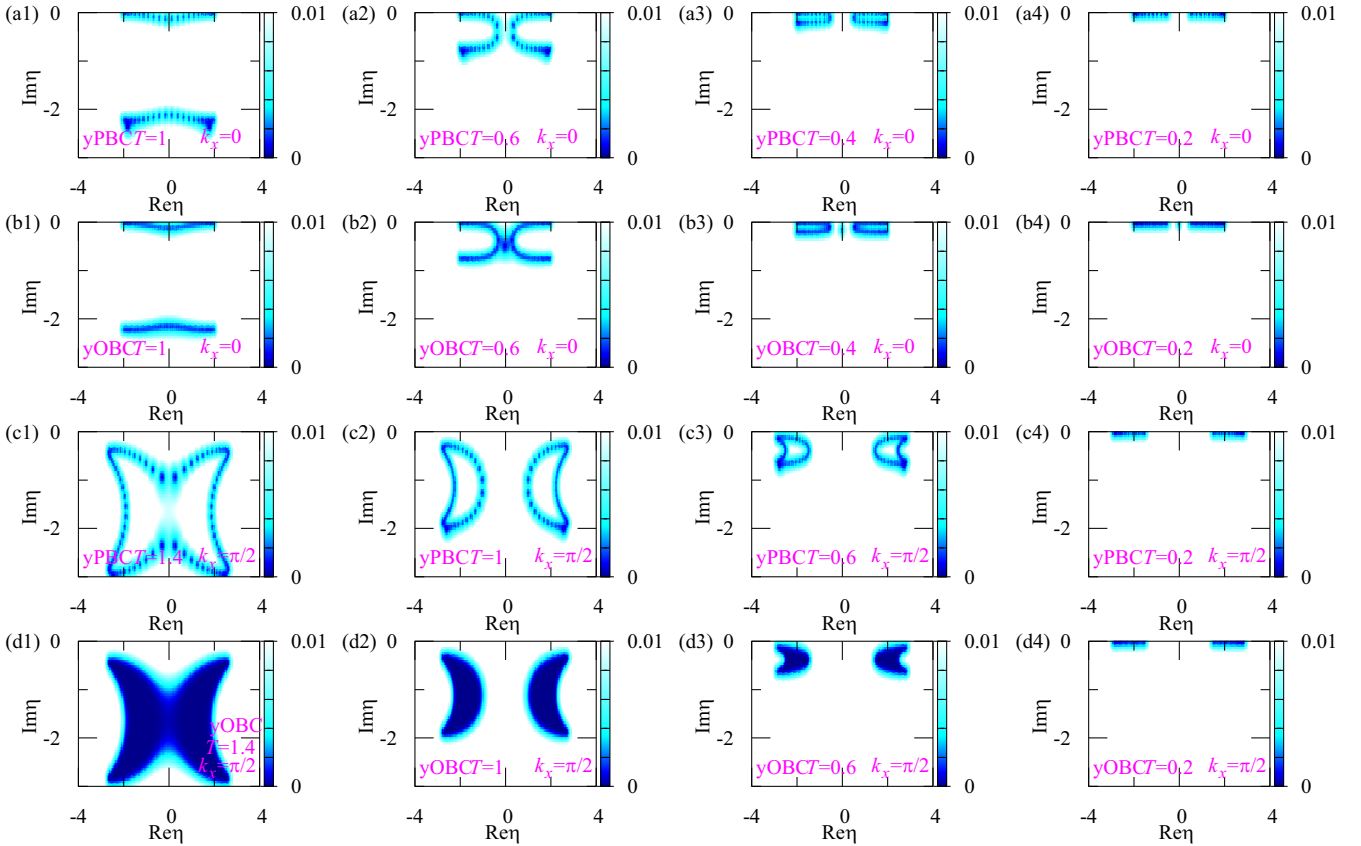


FIG. 2. Pseudospectrum of the effective Hamiltonian  $\hat{H}_{\text{eff}}(\omega = 0, k_x)$  for  $L_y = 50$  and  $U = 8$ . The color denotes the minimum singular value for a given  $\eta$ . Panels (a1)–(a4) and (b1)–(b4) [(c1)–(c4) and (d1)–(d4)] are the data for  $k_x = 0$  [ $k_x = \pi/2$ ]. Panels (a1)–(a4) and (c1)–(c4) [(b1)–(b4) and (d1)–(d4)] are obtained by imposing the yPBC [yOBC]. The data shown in panels (a1)–(a4) and (b1)–(b4) [(c1)–(c4) and (d1)–(d4)] are obtained for  $T = 1, 0.6, 0.4$ , and  $0.2$  [ $T = 1.4, 1, 0.6$ , and  $0.2$ ].

with a pseudoeigenvector  $\mathbf{v} \in \mathbb{C}^N$  satisfying  $\|\mathbf{v}\|_2 = 1$ . The symbol  $\|\mathbf{v}\|_2$  denotes the norm of a vector  $\mathbf{v}$ ;  $\|\mathbf{v}\|_2 := [\sum_j v_j v_j^*]^{1/2}$  with  $v_j^*$  being complex conjugation of the  $j$ th component of the vector  $\mathbf{v}$ . We stress that  $H_{\text{eff}}(\omega, k_x)$  depends on  $\omega$ , meaning that pseudoeigenvalues  $\eta$  also depend on  $\omega$ .

For computation of the  $\epsilon$ -pseudospectrum, applying the singular value decomposition is useful; the  $\epsilon$ -pseudospectrum can be computed by searching pseudoeigenvalues  $\eta \in \mathbb{C}$  satisfying

$$s_{\min}[\eta \mathbb{1} - \hat{H}_{\text{eff}}(\omega, k_x)] < \epsilon, \quad (6)$$

where  $s_{\min}(\hat{H}_{\text{eff}})$  denotes the minimum singular value of a non-Hermitian matrix  $\hat{H}_{\text{eff}}$ . The pseudoeigenvector is obtained from the unitary matrix of the singular value decomposition (see Appendix B).

The above two definitions of the pseudospectrum are equivalent [88], which is shown in Appendix B.

### III. R-DMFT RESULTS

In this section, after a brief discussion of the DOS, we see that  $\hat{H}_{\text{eff}}$  shows the skin effect because of the nontrivial point-gap topology [for a definition of the point gap, see Eq. (7)]. Our R-DMFT simulation demonstrates that the above point-gap topology induces additional pseudoeigenstates for

the yOBC. We also elucidate that additional pseudoeigenstates emerge due to the nontrivial line-gap topology [for a definition of the line gap, see Eq. (8)].

The above two types of gap are defined as follows. The point gap of given energy  $E_{\text{ref}} \in \mathbb{C}$  opens when

$$\varepsilon_n - E_{\text{ref}} \neq 0 \quad (7)$$

holds for  $n = 0, 1, \dots, \dim \hat{H}_{\text{eff}} - 1$ . Here,  $\varepsilon$ 's are the eigenvalues of  $\hat{H}_{\text{eff}}(\omega = 0, k_x)$ . When the point gap opens, the system may possess the corresponding nontrivial topology (i.e., point-gap topology) which induces the skin effect for non-Hermitian tight-binding models [33,35,36].

The line gap opens when

$$\text{Re } \varepsilon_n \neq 0 \quad (8)$$

holds for  $n = 0, 1, \dots, \dim \hat{H}_{\text{eff}} - 1$ . When the line gap opens, the system may possess the corresponding nontrivial topology (i.e., line-gap topology). As we see in Sec. III C, the nontrivial line-gap topology induces zero modes in finite-temperature regions [see just below Eq. (10)].

#### A. Density of states

Let us start with the noninteracting case. As the Bloch Hamiltonian  $\hat{h}(\mathbf{k})$  preserves the ‘‘sublattice’’ symmetry [89]

$[\hat{\tau}_1 \hat{h}(\mathbf{k}) \hat{\tau}_1 = -\hat{h}(\mathbf{k})]$ , the winding number may take a non-trivial value for a one-dimensional subsystem specified by  $k_x$ . Indeed, the winding number takes one for  $-\pi \leq k_x \lesssim -2.88$ ,  $-0.27 \lesssim k_x \lesssim 0.27$ , and  $-2.88 \lesssim k_x \leq \pi$  otherwise it takes zero. The nontrivial value of the winding number induces the zero-energy states.

These zero-energy states survive even in the presence of the Hubbard interaction  $U$ . For  $U = 8$ , the DOS  $\rho(\omega, k_x) = \frac{1}{L_y} \sum_{i_y, \alpha} [\hat{G}(\omega, k_x)]_{i_y, \alpha i_y, \alpha}$  is plotted in Figs. 1(a) and 1(b). For  $k_x = 0$  and the yOBC, the DOS shows a sharp peak at  $\omega = 0$  due to the edge states whereas such a peak cannot be observed for  $k_x = \pi/2$ . As discussed in Sec. III C, the emergence of the sharp peak can be more clearly understood in terms of the non-Hermitian topology whose topological invariant is a non-Hermitian extension of the winding number [see Eq. (10)].

### B. Eigenvalues of the effective Hamiltonian

Now, we discuss whether the effective Hamiltonian  $\hat{H}_{\text{eff}}(\omega, k_x) := \hat{h}(k_x) + \hat{\Sigma}(\omega + i\delta)$  exhibits the skin effect, i.e., extreme sensitivity to the boundary conditions of the spectrum and eigenvectors. As we see below, the effective Hamiltonian shows the skin effect for  $k_x = \pi/2$ . Figures 1(c) and 1(d) show the eigenvalues of  $\hat{H}_{\text{eff}}(\omega = 0, k_x)$  for  $k_x = 0$  and  $k_x = \pi/2$ , respectively. These figures show that in contrast to the case for  $k_x = 0$ , the spectrum for  $k_x = \pi/2$  shows significant dependence of the boundary condition. In addition, as shown in Fig. 1(e), almost all right eigenvectors  $|\psi_n\rangle_R$  ( $n = 0, 1, \dots, \dim \hat{H}_{\text{eff}} - 1$ ) are localized at  $i_y = 0$  for  $k_x = \pi/2$  and the yOBC.

The above significant dependence of the spectrum is consistent with the nontrivial value of the winding number  $W_P(k_x, E_{\text{ref}})$  of the point gap,

$$W_P(k_x, E_{\text{ref}}) = \int_{-\pi}^{\pi} \frac{dk_y}{2\pi i} \partial_{k_y} \ln \det[\hat{H}_{\text{eff}}(0, \mathbf{k}) - E_{\text{ref}} \mathbb{1}], \quad (9)$$

where  $E_{\text{ref}}$  denotes the reference energy. Figure 1(f) indicates that the winding number takes one at  $k_x = \pi/2$  where the skin effect is observed, whereas it takes zero at  $k_x = 0$ .

The above results, (i.e., the significant dependence of the eigenvalues, the winding number  $W_P$ , and the localization of eigenvectors), indicate that the effective Hamiltonian exhibits the skin effect for  $(\omega, k_x) = (0, \pi/2)$ . The similar behaviors of the energy spectrum and the localization can be observed as long as the winding number takes a nontrivial value.

So far, we have seen that for  $k_x = \pi/2$ , the point-gap topology of the effective Hamiltonian  $\hat{H}_{\text{eff}}(\omega = 0, k_x)$  becomes nontrivial and induces the skin effect [see Figs. 1(c)–1(e)], although the DOS does not show the corresponding extreme sensitivity to the boundary conditions [see Fig. 1(b)]. We note that this behavior is consistent [90] with the argument in Ref. [77].

### C. Pseudospectrum

As proposed by Ref. [77], the nontrivial value of the winding number  $W_P$ , characterizing the skin effect, is reflected in the the pseudospectrum. Figure 2 shows a pseudospectrum of  $\hat{H}_{\text{eff}}(\omega = 0, k_x)$ . Figures 2(a1)–2(a4) and 2(b1)–2(b4) are

the data for  $k_x = 0$  which we discuss in the latter half of this section.

Figures 2(c1)–2(c4) and 2(d1)–2(d4) indicate that the point-gap topology induces an additional structure of the pseudospectrum for the yOBC. In order to see this, let us note that for  $k_x = \pi/2$ , the winding number  $W_P(\pi/2, E_{\text{ref}})$  with  $E_{\text{ref}} = -2 + 0.5 \Sigma_{(L_y/2)b\uparrow}(\omega = 0)$  takes one for  $0 < T \lesssim 0.09$ . Figures 2(c1)–2(c4) show the pseudospectrum for  $k_x = \pi/2$  and the yPBC. These figures indicate that for the yPBC, the pseudospectrum shows a loop as the spectrum of  $\hat{H}_{\text{eff}}$  does. For the yOBC, the pseudospectrum shows additional structures; besides the loop structure observed for the yPBC, the area enclosed by the loops also becomes pseudoeigenvalues [see Figs. 2(d1)–2(d4)]. The above data indicate that the nontrivial topology of the point gap induces the edge states of the pseudospectrum.

We recall that the nontrivial point-gap topology is induced by finite temperatures; finite-temperature results in a finite lifetime of quasiparticles which is an origin of the loop structure of  $\hat{H}_{\text{eff}}(\omega = 0, k_x)$  [see Figs. 1(d) and 1(f)].

Besides the point gap, one may find a line gap, another type of gaps for non-Hermitian systems. Our numerical data show that the nontrivial topology of the line gap also affects the pseudospectrum [see Figs. 2(a1)–2(a4) and 2(b1)–2(b4)].

To see this, first, we introduce the winding number  $W_L(k_x)$  of the line gap. Because the non-Hermitian Hamiltonian preserves the sublattice symmetry  $\hat{\tau}_1 \hat{H}_{\text{eff}}(\omega, \mathbf{k}) \hat{\tau}_1 = -\hat{H}_{\text{eff}}(\omega, \mathbf{k})$ , the following winding number:

$$W_L(k_x) = \int_{-\pi}^{\pi} \frac{dk_y}{4\pi i} \text{tr}[\hat{\tau}_1 \hat{H}_{\text{eff}}^{-1}(0, \mathbf{k}) \partial_{k_y} \hat{H}_{\text{eff}}(0, \mathbf{k})] \quad (10)$$

is quantized as long as the line gap opens. For instance,  $W_L(0)$  takes one for  $T \lesssim 0.6$  and  $U = 8$ , whereas  $W_L(\pi/2)$  takes zero for  $T \lesssim 0.06$  and  $U = 8$ . As well as in the DOS [91] [see Fig. 1(a)], The nontrivial line-gap topology for  $k_x = 0$  is reflected in the pseudospectrum. Figures 2(a1)–2(a4) [2(b1)–2(b4)] show a pseudospectrum for  $k_x = 0$  and the yPBC [yOBC]. In the low-temperature region  $T \lesssim 0.6$ , the pseudospectrum shows a peak on the imaginary axis  $\text{Re } \eta = 0$  only for the yOBC [see Figs. 2(b3) and 2(b4)], which corresponds to the nontrivial topology of  $W_L(0)$ . Increasing the temperature closes the line-gap, and the peak located on the imaginary axis disappears [see Figs. 2(b1) and 2(b2)]. The above facts mean that additional pseudoeigenenergy is induced by the nontrivial line-gap topology which is destroyed by increasing the temperature.

So far, we have seen that temperatures affect the two types of topology in the opposite way; increasing the temperature makes the point-gap topology nontrivial, in contrast, it destroys the nontrivial topology of the line gap. This fact is also reflected in the following quantity:

$$A_{\text{ps}}(\omega) = \sum_{\{\eta(\omega)\}} \frac{1}{\omega + i\delta - \eta(\omega)}. \quad (11)$$

Here the summation is taken over all pseudoeigenvalues  $\eta(\omega)$  which are computed at each value of  $\omega$ . We call  $A_{\text{ps}}(\omega)$  the local pseudospectral weight because it is analogous to the local spectral weight [92,93]. In Figs. 3(a) and 3(b), the local pseudospectral weight is plotted for several values



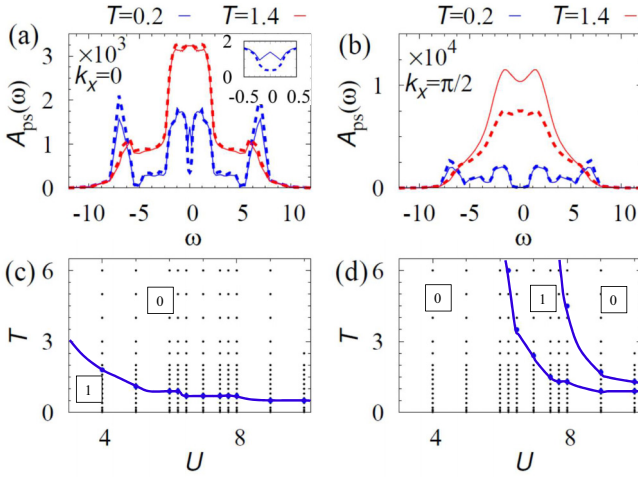


FIG. 3. (a) and (b) The local pseudospectral weight for several cases of the boundary conditions and temperatures. Panel (a) [(b)] shows the data for  $k_x = 0$  [ $k_x = \pi/2$ ]. These data are obtained for  $U = 8$ . (c) and (d) Phase diagrams of the interaction  $U$  vs temperature  $T$ . In panel (c) [(d)], numbers in squares indicate the values of  $W_L(k_x = 0)$  [ $W_p(k_x, E_{ref})$  with  $k_x = \frac{\pi}{2}$  and  $E_{ref} = -2 + 0.5\Sigma_{(L,\nu/2)b\uparrow}(i\delta)$ ]. We note that for  $U \leq 10$  the Mott transition is not observed. The system is half-filled for an arbitrary value of  $U$ .

of the temperature. Figure 3(a) indicates that only for low temperatures (e.g.,  $T = 0.01$ ),  $A_{ps}$  at  $k_x = 0$  changes depending on the boundary conditions, which is no longer observed for  $T = 0.07$ . Figure 3(b) indicates that for high temperatures (e.g.,  $T = 0.07$ )  $A_{ps}$  at  $k_x = \pi/2$  changes depending on the boundary conditions.

The above temperature effects are summarized in Figs. 3(c) and 3(d); the nontrivial topology of the line gap (the point gap) is destroyed by increasing (decreasing) the temperature.

#### IV. SUMMARY

By making use of the R-DMFT, we have analyzed the two-dimensional correlated system in equilibrium whose effective Hamiltonian exhibits the skin effect due to the nontrivial point-gap topology. As well as the DOS, we have also computed the pseudospectrum which was recently proposed in Ref. [77].

Our R-DMFT simulation has demonstrated that the above nontrivial point-gap topology induces additional pseudo-eigenstates for the yOBC in contrast to the dependence of the DOS on the boundary condition. We have further elucidated effects of the line-gap topology on the pseudospectrum. Our R-DMFT study has elucidated that in contrast to the point-gap topology, the damping of quasiparticles is harmful for the line-gap topology, which is reflected in temperature dependence of the local pseudospectral weight.

We consider that numerical simulations based on more accurate methods (e.g., methods based on the cluster DMFT [94,95] or a more accurate impurity solver, such as the numerical renormalization group [96–98] or continuous-time quantum Monte Carlo method [99–101]) should yield the essentially same results because the above non-Hermitian topological properties are independent of quantitative de-

tails of the self-energy. Namely, in the absence of the Mott transition, the renormalization factor (and the self-energy) continuously change by changing the interaction, although it depends on the impurity solvers how accurately the correlations are into account (see Fig. 1 of Ref. [102]). Thus, before Mott transition, the essentially same physics of the nontrivial point- (line-) gap topology is considered to be observed by employing more accurate results although the parameter region (e.g., interaction strength) shifts. We note, however, that it is also interesting to analyze the non-Hermitian topological properties in the Mott insulator, which is left an open question to be addressed.

We also note that although the relation of the pseudospectra and the angle-resolved photoemission spectroscopy has been discussed theoretically [77], the experimental observation has not been addressed yet, which is also left as a crucial open question to be addressed.

#### ACKNOWLEDGMENTS

This work was supported by JSPS Grant-in-Aid for Scientific Research on Innovative Areas “Discrete Geometric Analysis for Materials Design:” Grant No. JP20H04627. This work is also supported by JSPS KAKENHI Grant No. JP19K21032. The author thanks the Supercomputer Center, the Institute for Solid State Physics, University of Tokyo for the use of the facilities.

#### APPENDIX A: REMARKS OF THE PSEUDOSPECTRUM

The following facts are discussed in Ref. [88]. However, we summarize them in order to make the paper self-contained.

##### 1. Three definitions of the pseudospectrum

Consider an  $N \times N$  matrix  $\hat{A} \in \mathbb{C}^{N \times N}$ . Then, there exist three definitions of the  $\epsilon$ -pseudospectrum  $\sigma_\epsilon(\hat{A})$  with  $\epsilon > 0$ . Before the details, we define a 2-norm of a matrix,

$$\|\hat{A}\|_2 = \max_{\mathbf{v}} \frac{\|\hat{A}\mathbf{v}\|_2}{\|\mathbf{v}\|_2}. \quad (\text{A1})$$

We recall that  $\|\mathbf{v}\|_2$  denotes the norm of a vector  $\mathbf{v}$ ;  $\|\mathbf{v}\|_2 := [\sum_j v_j v_j^*]^{1/2}$  with  $v_j^*$  being the complex conjugation of the  $j$ th component of the vector  $\mathbf{v}$ .

In the following, we see the three definitions of the  $\epsilon$ -pseudospectrum.

*The first definition.* The  $\epsilon$ -pseudospectrum is a set of pseudo-eigenvalues  $\eta \in \mathbb{C}$  satisfying

$$\|[\eta \mathbb{1} - \hat{A}]^{-1}\|_2 > \epsilon^{-1}. \quad (\text{A2})$$

*The second definition.* The  $\epsilon$ -pseudospectrum is the set of eigenvalues  $\eta \in \mathbb{C}$  of the matrix  $\hat{A} + \hat{E}$  defined by a matrix  $\hat{E} \in \mathbb{C}^{N \times N}$  with  $\|\hat{E}\|_2 < \epsilon$ . Namely,  $\eta \in \mathbb{C}$  satisfies

$$(\hat{A} + \hat{E})\mathbf{v} = \eta\mathbf{v}, \quad (\text{A3})$$

with the eigenvector  $\mathbf{v}$  ( $\|\mathbf{v}\|_2 = 1$ ).

*The third definition.* This equation is the same as the one defined in Eq. (5); the  $\epsilon$ -pseudospectrum is the set of  $\eta \in \mathbb{C}$

satisfying

$$\|(\eta \mathbb{1} - \hat{A})\mathbf{v}\|_2 < \epsilon \quad (\text{A4})$$

for a normalized vector  $\mathbf{v}$  ( $\mathbf{v} \in \mathbb{C}^N$  and  $\|\mathbf{v}\|_2 = 1$ ).

In the next section, we prove the equivalence of these three definitions.

## 2. Equivalence of the three definitions

Based on the argument provided in Ref. [88] (in particular, see p. 16 of the textbook), we prove the equivalence of the above three definitions.

In the following, we address the proof by the following three steps.

(i) Eq. (A3)  $\Rightarrow$  Eq. (A4). Supposing that Eq. (A3) holds, we have Eq. (A4), which can be seen as follows.

Equation (A3) can be rewritten as

$$(\eta \mathbb{1} - \hat{A})\mathbf{v} = \hat{E}\mathbf{v}. \quad (\text{A5})$$

We note that the inequality  $\|\hat{E}\mathbf{v}\|_2 < \epsilon$  holds because  $\hat{E}$  satisfies  $\|\hat{E}\|_2 < \epsilon$ . Thus, we obtain

$$\|(\eta \mathbb{1} - \hat{A})\mathbf{v}\|_2 < \epsilon, \quad (\text{A6})$$

with a vector  $\mathbf{v}$  satisfying  $\|\mathbf{v}\|_2 = 1$ .

(ii) Eq. (A4)  $\Rightarrow$  Eq. (A2). Supposing that Eq. (A4) holds, we have Eq. (A2), which can be seen as follows. First, we note that Eq. (A4) indicates the relation,

$$\|(\eta \mathbb{1} - \hat{A})\mathbf{v}\|_2 = s < \epsilon, \quad (\text{A7})$$

with  $\mathbf{v} = 1$  and a non-negative number  $s \in \mathbb{R}$ . Thus, with a vector  $\mathbf{u} \in \mathbb{C}^N$  satisfying  $\|\mathbf{u}\|_2 = 1$ , we have

$$(\eta \mathbb{1} - \hat{A})\mathbf{v} = s\mathbf{u}, \quad (\text{A8})$$

which is further rewritten as

$$(\eta \mathbb{1} - \hat{A})^{-1}\mathbf{u} = s^{-1}\mathbf{v}. \quad (\text{A9})$$

Recalling Eq. (A1), we have

$$\|(\eta \mathbb{1} - \hat{A})^{-1}\|_2 \geq \|(\eta \mathbb{1} - \hat{A})^{-1}\mathbf{u}\|_2 = s^{-1} > \epsilon^{-1}. \quad (\text{A10})$$

Therefore, we obtain Eq. (A4) from Eq. (A2).

(iii) Eq. (A2)  $\Rightarrow$  Eq. (A3). Supposing that Eq. (A2) holds, we have Eq. (A3), which can be seen as follows.

Because Eq. (A1) holds, there exists  $\mathbf{u} \in \mathbb{C}^N$  satisfying

$$\|(\eta \mathbb{1} - \hat{A})\|_2 = \|(\eta \mathbb{1} - \hat{A})^{-1}\mathbf{u}\|_2 = s^{-1} > \epsilon^{-1}, \quad (\text{A11})$$

which results in

$$(\eta \mathbb{1} - \hat{A})^{-1}\mathbf{u} = s^{-1}\mathbf{v}. \quad (\text{A12})$$

This relation is further rewritten as

$$(\eta \mathbb{1} - \hat{A})\mathbf{v} = s\mathbf{u}. \quad (\text{A13})$$

Because  $s\mathbf{u} = \hat{E}\mathbf{v}$  ( $\hat{E} := s\mathbf{u}\mathbf{v}^\dagger$ ) holds, we have

$$(\eta \mathbb{1} - \hat{A})\mathbf{v} = \hat{E}\mathbf{v}. \quad (\text{A14})$$

Noting that  $\|\hat{E}\|_2 = \|s\mathbf{u}\mathbf{v}^\dagger\|_2 = s < \epsilon$ , we obtain Eq. (A3).

Putting the above arguments (i)–(iii) together, we end up with the equivalence of the three definitions.

## APPENDIX B: PROOF OF EQ. (6)

### 1. Eq. (5) $\Leftrightarrow$ Eq. (6)

Supposing that Eq. (5) holds, we have Eq. (6), which can be seen as follows.

First, we apply the singular value decomposition,

$$\eta \mathbb{1} - \hat{H}_{\text{eff}} = \hat{U} \hat{\Lambda} \hat{V}, \quad (\text{B1})$$

where  $\hat{U}$  and  $\hat{V}$  are unitary matrices and  $\hat{\Lambda}$  is a diagonal matrix whose diagonal elements  $\lambda_i \in \mathbb{R}$  ( $i = 1, 2, \dots, N$ ) are non-negative.

Thus, the left-hand side of Eq. (5) is rewritten as

$$\begin{aligned} \|(\eta \mathbb{1} - \hat{H}_{\text{eff}})\mathbf{v}\|_2 &= (\mathbf{v}^\dagger \hat{V}^\dagger \hat{\Lambda} \hat{U}^\dagger \hat{U} \hat{\Lambda} \hat{V} \mathbf{v})^{1/2} \\ &= (\mathbf{v}^\dagger \hat{V}^\dagger \hat{\Lambda}^2 \hat{V} \mathbf{v})^{1/2} \\ &= \left( \sum_j |v_j|^2 \lambda_j^2 \right)^{1/2}, \end{aligned} \quad (\text{B2})$$

where  $v'_j$  is defined as  $v'_j := \sum_i V_{ji} v_i$ .

The above facts indicate that  $\eta$  is an  $\epsilon$ -pseudoeigenvalue ( $\epsilon > 0$ ) when

$$s_{\min}(\eta \mathbb{1} - \hat{H}_{\text{eff}}) < \epsilon \quad (\text{B3})$$

is satisfied. Here,  $s_{\min}(\eta \mathbb{1} - \hat{H}_{\text{eff}})$  denotes the minimum of the singular values  $\lambda$ 's.

Therefore, we obtain Eq. (6). Equation (B2) also indicates that the pseudoeigenvector  $\mathbf{v}$  is given by  $v_j = (V^\dagger)_{j1}$ .

### 2. Another proof

Equation (6) can also be proven from Eq. (A1). This can be seen by noting the following fact: for an arbitrary matrix  $\hat{B} \in \mathbb{C}^{N \times N}$ :

$$\|\hat{B}\|_2 = s_{\max}(\hat{B}), \quad (\text{B4})$$

where  $s_{\max}(\hat{B})$  is the maximum singular value of a  $N \times N$  matrix  $\hat{B} \in \mathbb{C}^{N \times N}$ .

With Eq. (B4), we obtain

$$\begin{aligned} \|[\eta \mathbb{1} - \hat{H}_{\text{eff}}]^{-1}\|_2 &= s_{\max}([\eta \mathbb{1} - \hat{H}_{\text{eff}}]^{-1}) \\ &= [s_{\min}(\eta \mathbb{1} - \hat{H}_{\text{eff}})]^{-1}. \end{aligned} \quad (\text{B5})$$

Combining the above equation and Eq. (A2) results in Eq. (6).

In the following, we prove Eq. (B4). First, we note that with the singular value decomposition ( $\hat{B} := \hat{U}_B \hat{\Lambda}_B \hat{V}_B$ ), we have

$$\begin{aligned} \|\hat{B}\mathbf{v}\|_2 &= \sqrt{\mathbf{v}^\dagger \hat{B}^\dagger \hat{B} \mathbf{v}} \\ &= \sqrt{\mathbf{v}^\dagger \hat{V}_B^\dagger \hat{\Lambda}_B \hat{U}_B^\dagger \hat{U}_B \hat{\Lambda}_B \hat{V}_B \mathbf{v}} \\ &= \sqrt{\mathbf{v}^\dagger \hat{V}_B^\dagger \hat{\Lambda}_B^2 \hat{V}_B \mathbf{v}}. \end{aligned} \quad (\text{B6})$$

Here  $\hat{U}_B$  and  $\hat{V}_B$  are unitary matrices, and  $\hat{\Lambda}_B$  is a diagonal matrix whose diagonal elements  $\lambda_{Bi}$  ( $i = 1, 2, \dots, N$ ) are singular values of  $\hat{B}$ . The vector  $\mathbf{v}$  is an arbitrary vector  $\mathbf{v} \in \mathbb{C}^N$ .

By making use of Eq. (B6), we obtain Eq. (B4),

$$\begin{aligned} \|\hat{B}\|_2 &= \max_n \|\hat{B}\mathbf{n}\|_2 \\ &= \max_n \sqrt{\mathbf{n}^\dagger \hat{V}_B^\dagger \hat{\Lambda}_B^2 \hat{V}_B \mathbf{n}} \end{aligned}$$

$$\begin{aligned}
 &= \max_{\mathbf{n}'} \sqrt{\mathbf{n}'^\dagger \hat{\Lambda}_B^2 \mathbf{n}'} \\
 &= \max_{\mathbf{n}'} \left( \sum_j |\mathbf{n}'|_{Bj}^2 \lambda_{Bj}^2 \right)^{1/2} \\
 &= s_{\max}(\hat{B}), \tag{B7}
 \end{aligned}$$

where we have defined a vector  $\mathbf{n}' := \hat{V} \mathbf{n}$  satisfying  $\|\mathbf{n}'\|_2 = 1$ . Thus, we obtain Eq. (B4).

As discussed above, we can also obtain Eq. (6) starting from Eq. (A1).

### APPENDIX C: SELF-ENERGY

Here, we plot the self-energy  $\Sigma_{i_y, b\uparrow}(\omega)$  which is used for computation of the pseudospectrum.

Figure 4 is the data for  $i_y = 0, 1, 2, 24$ ,  $L_y = 50$ , and  $U = 8$ . Figures 4(b) and 4(d) indicate that the imaginary part does not diverge, meaning that the interaction strength  $U = 8$  is smaller than the critical value of the Mott transition.

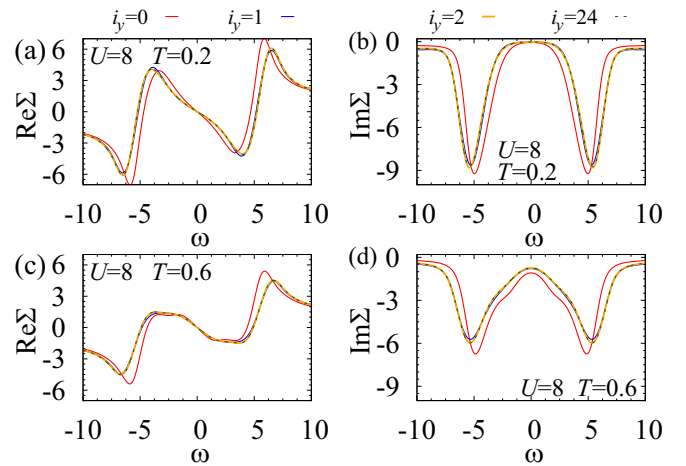


FIG. 4. (a) [(b)] The real (imaginary) part of the self-energy  $\Sigma_{i_y, b\uparrow}(\omega)$  for  $U = 8$  and  $T = 0.2$ . (c) [(d)] The real (imaginary) part of the self-energy  $\Sigma_{i_y, b\uparrow}(\omega)$  for  $U = 8$  and  $T = 0.6$ . These data are obtained under the yOBC. We note that data for  $i_y = 0, 1$  deviate from those of the bulk, whereas data for  $i_y \geq 2$  are almost the same as those of the bulk.

- [1] C. L. Kane and E. J. Mele, *Phys. Rev. Lett.* **95**, 146802 (2005).
- [2] C. L. Kane and E. J. Mele, *Phys. Rev. Lett.* **95**, 226801 (2005).
- [3] B. A. Bernevig, T. L. Hughes, and S.-C. Zhang, *Science* **314**, 1757 (2006).
- [4] M. König, S. Wiedmann, C. Brüne, A. Roth, H. Buhmann, L. W. Molenkamp, X.-L. Qi, and S.-C. Zhang, *Science* **318**, 766 (2007).
- [5] X.-L. Qi, T. L. Hughes, and S.-C. Zhang, *Phys. Rev. B* **78**, 195424 (2008).
- [6] M. Z. Hasan and C. L. Kane, *Rev. Mod. Phys.* **82**, 3045 (2010).
- [7] X.-L. Qi and S.-C. Zhang, *Rev. Mod. Phys.* **83**, 1057 (2011).
- [8] N. Hatano and D. R. Nelson, *Phys. Rev. Lett.* **77**, 570 (1996).
- [9] Y. C. Hu and T. L. Hughes, *Phys. Rev. B* **84**, 153101 (2011).
- [10] K. Esaki, M. Sato, K. Hasebe, and M. Kohmoto, *Phys. Rev. B* **84**, 205128 (2011).
- [11] T. E. Lee, *Phys. Rev. Lett.* **116**, 133903 (2016).
- [12] F. K. Kunst, E. Edvardsson, J. C. Budich, and E. J. Bergholtz, *Phys. Rev. Lett.* **121**, 026808 (2018).
- [13] E. Edvardsson, F. K. Kunst, and E. J. Bergholtz, *Phys. Rev. B* **99**, 081302(R) (2019).
- [14] Z. Gong, Y. Ashida, K. Kawabata, K. Takasan, S. Higashikawa, and M. Ueda, *Phys. Rev. X* **8**, 031079 (2018).
- [15] K. Kawabata, K. Shiozaki, M. Ueda, and M. Sato, *Phys. Rev. X* **9**, 041015 (2019).
- [16] H. Zhou and J. Y. Lee, *Phys. Rev. B* **99**, 235112 (2019).
- [17] K. Yokomizo and S. Murakami, *Phys. Rev. Lett.* **123**, 066404 (2019).
- [18] N. Okuma and M. Sato, *Phys. Rev. Lett.* **123**, 097701 (2019).
- [19] K. Yokomizo and S. Murakami, *Phys. Rev. Research* **2**, 043045 (2020).
- [20] E. J. Bergholtz, J. C. Budich, and F. K. Kunst, *Rev. Mod. Phys.* **93**, 015005 (2021).
- [21] T. Yoshida, R. Peters, N. Kawakami, and Y. Hatsugai, *Prog. Theor. Exp. Phys.* **2020**, 12A109 (2020).
- [22] Y. Ashida, Z. Gong, and M. Ueda, *arXiv:2006.01837*.
- [23] H. Shen, B. Zhen, and L. Fu, *Phys. Rev. Lett.* **120**, 146402 (2018).
- [24] Y. Xu, S.-T. Wang, and L.-M. Duan, *Phys. Rev. Lett.* **118**, 045701 (2017).
- [25] J. C. Budich, J. Carlström, F. K. Kunst, and E. J. Bergholtz, *Phys. Rev. B* **99**, 041406(R) (2019).
- [26] R. Okugawa and T. Yokoyama, *Phys. Rev. B* **99**, 041202(R) (2019).
- [27] T. Yoshida, R. Peters, N. Kawakami, and Y. Hatsugai, *Phys. Rev. B* **99**, 121101(R) (2019).
- [28] H. Zhou, J. Y. Lee, S. Liu, and B. Zhen, *Optica* **6**, 190 (2019).
- [29] K. Kawabata, T. Bessho, and M. Sato, *Phys. Rev. Lett.* **123**, 066405 (2019).
- [30] V. M. Martinez Alvarez, J. E. Barrios Vargas, and L. E. F. Foa Torres, *Phys. Rev. B* **97**, 121401(R) (2018).
- [31] S. Yao and Z. Wang, *Phys. Rev. Lett.* **121**, 086803 (2018).
- [32] S. Yao, F. Song, and Z. Wang, *Phys. Rev. Lett.* **121**, 136802 (2018).
- [33] C. H. Lee and R. Thomale, *Phys. Rev. B* **99**, 201103(R) (2019).
- [34] D. S. Borgnia, A. J. Kruchkov, and R.-J. Slager, *Phys. Rev. Lett.* **124**, 056802 (2020).
- [35] K. Zhang, Z. Yang, and C. Fang, *Phys. Rev. Lett.* **125**, 126402 (2020).
- [36] N. Okuma, K. Kawabata, K. Shiozaki, and M. Sato, *Phys. Rev. Lett.* **124**, 086801 (2020).
- [37] N. Okuma and M. Sato, *Phys. Rev. B* **102**, 014203 (2020).
- [38] S. Mu, C. H. Lee, L. Li, and J. Gong, *Phys. Rev. B* **102**, 081115(R) (2020).
- [39] C. H. Lee, *arXiv:2006.01182*.

- [40] R. Okugawa, R. Takahashi, and K. Yokomizo, *Phys. Rev. B* **102**, 241202 (2020).
- [41] K. Kawabata, M. Sato, and K. Shiozaki, *Phys. Rev. B* **102**, 205118 (2020).
- [42] Y. Fu, J. Hu, and S. Wan, *Phys. Rev. B* **103**, 045420 (2021).
- [43] C. E. Rüter, K. G. Makris, R. El-Ganainy, D. N. Christodoulides, M. Segev, and D. Kip, *Nat. Phys.* **6**, 192 (2010).
- [44] A. Regensburger, C. Bersch, M.-A. Miri, G. Onishchukov, D. N. Christodoulides, and U. Peschel, *Nature (London)* **488**, 167 (2012).
- [45] B. Zhen, C. W. Hsu, Y. Igarashi, L. Lu, I. Kaminer, A. Pick, S.-L. Chua, J. D. Joannopoulos, and M. Soljačić, *Nature (London)* **525**, 354 (2015).
- [46] A. U. Hassan, B. Zhen, M. Soljačić, M. Khajavikhan, and D. N. Christodoulides, *Phys. Rev. Lett.* **118**, 093002 (2017).
- [47] H. Zhou, C. Peng, Y. Yoon, C. W. Hsu, K. A. Nelson, L. Fu, J. D. Joannopoulos, M. Soljačić, and B. Zhen, *Science* **359**, 1009 (2018).
- [48] K. Takata and M. Notomi, *Phys. Rev. Lett.* **121**, 213902 (2018).
- [49] T. Ozawa, H. M. Price, A. Amo, N. Goldman, M. Hafezi, L. Lu, M. C. Rechtsman, D. Schuster, J. Simon, O. Zilberberg, and I. Carusotto, *Rev. Mod. Phys.* **91**, 015006 (2019).
- [50] L. Xiao, T. Deng, K. Wang, G. Zhu, Z. Wang, W. Yi, and P. Xue, *Nat. Phys.* **16**, 761 (2020).
- [51] S. Diehl, E. Rico, M. A. Baranov, and P. Zoller, *Nat. Phys.* **7**, 971 (2011).
- [52] C.-E. Bardyn, M. A. Baranov, C. V. Kraus, E. Rico, A. İmamoğlu, P. Zoller, and S. Diehl, *New J. Phys.* **15**, 085001 (2013).
- [53] A. Rivas, O. Viyuela, and M. A. Martin-Delgado, *Phys. Rev. B* **88**, 155141 (2013).
- [54] J. C. Budich, P. Zoller, and S. Diehl, *Phys. Rev. A* **91**, 042117 (2015).
- [55] J. C. Budich and S. Diehl, *Phys. Rev. B* **91**, 165140 (2015).
- [56] Z. Gong, S. Higashikawa, and M. Ueda, *Phys. Rev. Lett.* **118**, 200401 (2017).
- [57] S. Lieu, M. McGinley, and N. R. Cooper, *Phys. Rev. Lett.* **124**, 040401 (2020).
- [58] T. Yoshida, K. Kudo, and Y. Hatsugai, *Sci. Rep.* **9**, 16895 (2019).
- [59] T. Yoshida, K. Kudo, H. Katsura, and Y. Hatsugai, *Phys. Rev. Research* **2**, 033428 (2020).
- [60] T. Yoshida and Y. Hatsugai, *Phys. Rev. B* **100**, 054109 (2019).
- [61] A. Ghatak, M. Brandenbourger, J. van Wezel, and C. Coulais, *Natl. Ac. Sc. USA* **117**, 29561 (2020).
- [62] C. Scheibner, W. T. M. Irvine, and V. Vitelli, *Phys. Rev. Lett.* **125**, 118001 (2020).
- [63] T. Helbig, T. Hofmann, S. Imhof, M. Abdelghany, T. Kiessling, L. W. Molenkamp, C. H. Lee, A. Szameit, M. Greiter, and R. Thomale, *Nat. Phys.* **16**, 747 (2020).
- [64] T. Hofmann, T. Helbig, F. Schindler, N. Salgo, M. Brzezińska, M. Greiter, T. Kiessling, D. Wolf, A. Vollhardt, A. Kabašić *et al.*, *Phys. Rev. Research* **2**, 023265 (2020).
- [65] T. Yoshida, T. Mizoguchi, and Y. Hatsugai, *Phys. Rev. Research* **2**, 022062(R) (2020).
- [66] V. Kozii and L. Fu, [arXiv:1708.05841](https://arxiv.org/abs/1708.05841).
- [67] T. Yoshida, R. Peters, and N. Kawakami, *Phys. Rev. B* **98**, 035141 (2018).
- [68] H. Shen and L. Fu, *Phys. Rev. Lett.* **121**, 026403 (2018).
- [69] A. A. Zyuzin and A. Y. Zyuzin, *Phys. Rev. B* **97**, 041203(R) (2018).
- [70] M. Papaj, H. Isobe, and L. Fu, *Phys. Rev. B* **99**, 201107(R) (2019).
- [71] K. Kimura, T. Yoshida, and N. Kawakami, *Phys. Rev. B* **100**, 115124 (2019).
- [72] T. Matsushita, Y. Nagai, and S. Fujimoto, *Phys. Rev. B* **100**, 245205 (2019).
- [73] Y. Michishita, T. Yoshida, and R. Peters, *Phys. Rev. B* **101**, 085122 (2020).
- [74] Y. Michishita and R. Peters, *Phys. Rev. Lett.* **124**, 196401 (2020).
- [75] R. Rausch, R. Peters, and T. Yoshida, *New J. Phys.* **23**, 013011 (2021).
- [76] T. Matsushita, Y. Nagai, and S. Fujimoto, [arXiv:2004.11014](https://arxiv.org/abs/2004.11014).
- [77] N. Okuma and M. Sato, [arXiv:2008.06498](https://arxiv.org/abs/2008.06498).
- [78] A. Masuyama and T. Mutou, *J. Phys. Soc. Jpn.* **89**, 044708 (2020).
- [79] In addition, numerical data in Ref. [78] indicate that unless the Mott transition is absent, the interaction of orbital  $a$  just induces quantitative difference. Thus, as long as the Mott transition is absent, introducing the interaction of orbital  $a$  just results in quantitative difference.
- [80] M. Fujita, K. Wakabayashi, K. Nakada, and K. Kusakabe, *J. Phys. Soc. Jpn.* **65**, 1920 (1996).
- [81] W. Metzner and D. Vollhardt, *Phys. Rev. Lett.* **62**, 324 (1989).
- [82] E. Müller-Hartmann, *Z. Phys. B: Condens. Matter* **74**, 507 (1989).
- [83] A. Georges, G. Kotliar, W. Krauth, and M. J. Rozenberg, *Rev. Mod. Phys.* **68**, 13 (1996).
- [84] A. Georges and G. Kotliar, *Phys. Rev. B* **45**, 6479 (1992).
- [85] X. Y. Zhang, M. J. Rozenberg, and G. Kotliar, *Phys. Rev. Lett.* **70**, 1666 (1993).
- [86] H. Kajueter and G. Kotliar, *Phys. Rev. Lett.* **77**, 131 (1996).
- [87] In Ref. [77], the relevance of the pseudospectrum to the angle-resolved photoemission spectroscopy has been pointed out by analyzing the effects of non-Hermiticity on the photocurrent based on liner-response theory.
- [88] L. N. Trefethen and M. Embree, *Spectra and Pseudospectra: The Behavior of Nonnormal Matrices and Operators* (Princeton University Press, Princeton, NJ, 2005).
- [89] The symmetry constraint is called sublattice symmetry in Ref. [15]. We, thus, follow this notation although our system does not have sublattice;  $\alpha = a, b$  denotes orbital.
- [90] Reference [77] has analytically shown that the DOS is not sensitive to the boundary conditions even when  $H_{\text{eff}}$  shows skin effects. Here, we briefly describe the argument. The density of state is obtained by summing up the eigenvalues and eigenstates labeled by the momentum [under the open boundary condition, the momentum is defined on the complex plane (see Ref. [17])]. By using the residue theorem, one can see that the extreme sensitivity of the boundary condition vanishes due to the summation.



- [91] The fact that  $W_L$  predicts the presence/absence of the zero modes around the boundary can be understood by noting the following fact. Suppose that the line gap opens while approaching  $T = 0$  from a finite-temperature region. Then,  $W_L$  computed in a finite-temperature region is reduced to the ordinary winding number for a Hermitian matrix which predicts the presence/absence of the edge mode at  $T = 0$ .
- [92] D. Schuricht, S. Andergassen, and V. Meden, *J. Phys.: Condens. Matter* **25**, 014003 (2012).
- [93] The local spectral weight, or the local density of states, is defined as Ref. [92]  $A(\omega) = \frac{1}{\sqrt{L_x L_y}} \sum_{\mathbf{k}, \alpha} e^{i\mathbf{k} \cdot (\mathbf{R} - \mathbf{R}')} \frac{1}{\omega + i\delta - E_\alpha(\omega, \mathbf{k})}$  where  $E_\alpha(\omega, \mathbf{k})$  is the eigenvalues of the effective Hamiltonian  $\hat{H}(\omega, \mathbf{k})$ . The vectors  $\mathbf{R}$  and  $\mathbf{R}'$  specify the sites of the lattice.
- [94] G. Kotliar, S. Y. Savrasov, G. Pálsson, and G. Biroli, *Phys. Rev. Lett.* **87**, 186401 (2001).
- [95] T. Maier, M. Jarrell, T. Pruschke, and M. H. Hettler, *Rev. Mod. Phys.* **77**, 1027 (2005).
- [96] K. G. Wilson, *Rev. Mod. Phys.* **47**, 773 (1975).
- [97] R. Peters, T. Pruschke, and F. B. Anders, *Phys. Rev. B* **74**, 245114 (2006).
- [98] R. Bulla, T. A. Costi, and T. Pruschke, *Rev. Mod. Phys.* **80**, 395 (2008).
- [99] P. Werner, A. Comanac, L. de' Medici, M. Troyer, and A. J. Millis, *Phys. Rev. Lett.* **97**, 076405 (2006).
- [100] P. Werner and A. J. Millis, *Phys. Rev. B* **74**, 155107 (2006).
- [101] K. Haule, *Phys. Rev. B* **75**, 155113 (2007).
- [102] R. Bulla, *Phys. Rev. Lett.* **83**, 136 (1999).